Dynamic structural disorder in cristobalite: neutron total scattering measurement and reverse Monte Carlo modelling

Matthew G Tucker[1]**, Matthew P Squires**[1]**, Martin T Dove**[1,3] **and David A Keen**[2]

[1] Mineral Physics Group, Department of Earth Sciences, University of Cambridge, Downing Street, Cambridge CB2 3EQ, UK
[2] ISIS Facility, Rutherford Appleton Laboratory, Chilton, Didcot, Oxfordshire OX11 0QX, UK

E-mail: mtuc98@esc.cam.ac.uk (M G Tucker), martin@esc.cam.ac.uk (M T Dove) and d.a.keen@rl.ac.uk (D A Keen)

Abstract

The atomic structure of cristobalite in both its high-temperature β-phase and low-temperature α-phase has been studied using constrained reverse Monte Carlo modelling of neutron total scattering data. The modelling has shown that the disorder of the β-phase involves rotations and displacements of rigid SiO_4 tetrahedra, consistent with the predictions of the 'rigid-unit mode' (RUM) model. The structure of the α-phase is significantly different from that of the β-phase, but still has a degree of disorder. The calculated distribution of oxygen atoms in β-cristobalite is continuous rather than based on specific crystallographic sites. There is no evidence for correlations between the Si–O distance and the corresponding Si–O–Si bond angles, contrary to quantum mechanical calculation findings. The three-dimensional diffuse scattering has been calculated from the model configurations, and is found to be in agreement with experimental electron diffraction measurements and the predictions of the RUM model. There is little significant temperature dependence of the structure or diffuse scattering in the β-phase.

(Some figures in this article are in colour only in the electronic version; see `www.iop.org`)

1. Introduction

Silica, SiO_2, is one of the most important materials for a variety of reasons. It is important for geology as a component of the Earth, its glass phase is important as a ceramic, and its quartz phase is one of the most important piezoelectric materials. Moreover, the displacive phase transitions in the crystalline polymorphs are excellent prototype systems for general solid-state physics and chemistry investigations [1].

[3] Author to whom any correspondence should be addressed.

The cristobalite polymorph of silica has received a lot of attention over many years [2–11], in part because a number of other materials have structures based on that of cristobalite. There is a first-order phase transition at around 590 K between the high-temperature β-phase of cubic symmetry (space group $Fd\bar{3}m$) and the low-temperature α-phase of tetragonal symmetry (space group $P4_12_12$). There is a significant change in volume at the phase transition [6].

The structure of β-cristobalite has presented significant challenges to our understanding of the balance between short-range and long-range order. The structure defined by the average positions of the atoms is most easily described as derived from that of elemental silicon (fcc, with Si fractional coordinates $\pm(1/8, 1/8, 1/8)$), with an oxygen position half-way along each nearest-neighbour Si–Si vector. This is shown in figure 1(a). The problem with this structure is that it has straight Si–O–Si bonds, and it is known that in almost all silicate materials this bond has an angle between 145 and 150°. Related to this is the problem that the distance between the mean Si and O positions (1.55 Å [10]) is substantially lower than the usual Si–O bond length (1.61 Å). Moreover, the displacement parameters from crystal structure refinements (shown in figure 1(a) and discussed later) have the distribution of oxygen atoms spread out normal to the Si–Si vector [6], and the structure can be reconciled with a model with disordered orientations of the Si–O bonds to give an Si–O–Si angle close to 145° and an Si–O bond length close to typical values [9]. There have been attempts to refine the crystal structure assuming disordered positions for the oxygen atoms distributed on an annulus around the mean oxygen position. The most common approach is to assign six positions for each oxygen atom in a ring around its average position, each with 1/6 occupancy [6], as shown in figure 1(b). Although this model is more realistic than the ideal model with the oxygen actually located at its mean position—for example, as we demonstrate below, it gives more realistic Si–O bond distances, and it gives good agreement with experimental data in the crystal structure refinements—it
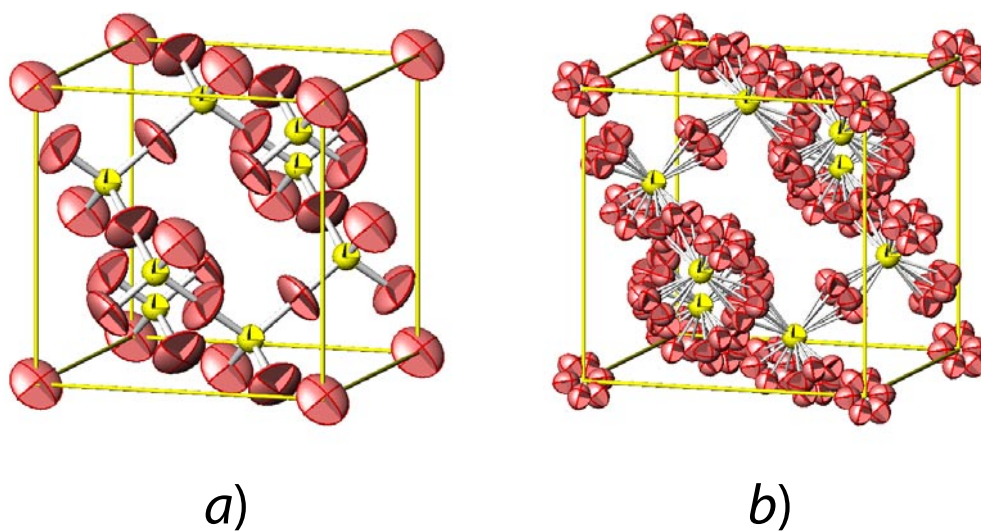

a)   b)

Figure 1. (a) The crystal structure of β-cristobalite refined using a single-site model for the oxygen atoms. (b) The crystal structure of β-cristobalite refined using the six-site model for the oxygen atoms. Both structures have the thermal displacement parameters represented by ellipsoids. In the single-site model, the thermal displacement ellipsoids of the oxygen atoms are elongated in the directions normal to the nearest-neighbour Si–Si vectors. In the six-site model, the thermal displacement ellipsoids of the oxygen atoms in a small ring overlap.

is quite possible that this model is still an oversimplification of the actual crystal structure of β-cristobalite. Moreover, as we will discuss in more detail below, the spatial resolution given by conventional diffraction measurements is coarser than the distances between the split sites (around 0.5 Å), which means that conventional diffraction techniques are not able to unambiguously discriminate between models of the disorder of the SiO_4 tetrahedra, simply because it is not possible with conventional diffraction to provide information about the spatial distribution of atoms to a sufficiently fine resolution.

The main question that is posed by the structure of β-cristobalite is how this disorder can be sustained. It has to be remembered that any Si–O bond is part of a SiO_4 tetrahedral unit, and these are not readily deformed by any significant amount. The tetrahedra are all linked into an infinite network through sharing of vertices. Thus the orientation of an Si–O bond is correlated with the rotation of the whole SiO_4 tetrahedron, and the rotation of one tetrahedron is correlated with the rotations of the tetrahedra linked to it. Thus the network may, at least in principle, be highly constrained, and the motions of the SiO_4 tetrahedra are controlled by the flexibility of the network. One popular explanation as to how the network would sustain orientational disorder of the Si–O bonds is to assume that the cubic structure is only an average over small domains of a lower-symmetry structure, one that has bent Si–O–Si bonds and Si–O bonds that have usual lengths. One obvious candidate structure is that of the tetragonal α-phase, space group $P4_12_12$ [5]. There are 12 orientations of a domain of this phase, and by having all domains present the cubic structure is an average of all domain orientations. An older model [12] has a different structure for the domains, with space group $I\bar{4}2d$. The general domain model is now known to be too simple, but it gives an idea of what it possible.

The alternative approach to understanding the nature of the structure of β-cristobalite is through the 'rigid-unit mode' model [13–16]. The important point in this model is that a structure made of a framework of linked polyhedra can have phonon modes in which the polyhedra move without distorting. The most familiar example of such a phonon, which we call a 'rigid-unit mode' (RUM), is the octahedral tilting soft mode in cubic perovskites such as $SrTiO_3$. An algorithm has been developed to facilitate the calculation of the RUMs for a given crystal structure at any given wave vector k, using a technique called the 'split-atom method' together with the formalism of molecular lattice dynamics [13, 17]. Calculations for β-cristobalite have shown that there is one RUM for every wave vector of the form $k = \{\xi, \xi, \zeta\}^*$, which lie in the $\langle 1, \bar{1}, 0 \rangle$ zones of reciprocal space [7, 8, 13, 14]. The distortion to give the crystal structure of α-cristobalite involves a RUM at $k = (1, 0, 0)$, which is doubly degenerate because this wave vector sits at the intersection of two planes of RUMs. Moreover, the alternative domain proposed for the $I\bar{4}2d$ modification of β-cristobalite is obtained by a distortion involving the triply degenerate RUM at $k = 0$, where there is an intersection of three planes of RUMs. Therefore both types of domain can exist as phonon fluctuations of β-cristobalite, but so also can all the distortions associated with the other RUMs in the $\langle 1, \bar{1}, 0 \rangle$ zones in reciprocal space. The upshot of this thinking is that the dynamic superposition of all RUMs can create a dynamically disordered structure. This point has been documented in some detail [8, 14].

The key to understanding local structure is through measurements of total scattering, $S(Q)$ [18–21]. In this approach, measurements are made of the total scattering of neutrons or x-rays, integrated over all energies, as a function of scattering vector Q. The total scattering signal contains both the Bragg elastic scattering, which gives the average structure, and the diffuse scattering. As we will discuss formally below, the Fourier transform of the total scattering signal gives the pair distribution functions, which contain information about the structure on a short length scale. This gives the ability to determine short-range fluctuations of

the crystal structure. Neutron total scattering measurements performed at a spallation source, which produces a rich spectrum of high-energy neutrons, can yield $S(Q)$ data up to large values of Q. For example, the data used in this paper were obtained for values of Q up to $Q_{max} = 50\,\text{Å}^{-1}$, which gives a spatial resolution of $\Delta r = 2\pi/Q_{max} = 0.13\,\text{Å}$. By comparison, the best spatial resolution that could be obtained using Cu Kα x-radiation would be 0.77 Å. Although atomic coordinates, and hence distances between mean positions, can be determined with a much greater precision in crystal structure refinement from conventional diffraction data, these are still subject to the constraints of the resolution. What is actually being refined is the mean position of a peak in the model atomic density function. In a well-ordered structure, the resolution does not cause a problem: the atoms are separated by distances greater than the intrinsic resolution, and it is still possible to determine the peak position with higher precision that the resolution. However, in disordered crystals where peaks in the density function are closer together than the intrinsic resolution, the detailed shape of the density function may be difficult to determine unambiguously, and hence different models may give fits to the data with more-or-less equal quality.

Previously we reported measurements of $S(Q)$ for cristobalite at several temperatures [10]. Analysis of the pair distribution functions gave a number of important results. *First*, we showed that the actual Si–O bond length obtained from the pair distribution functions is longer than the distance between the mean positions in the idealized structure, and similar in value to that in other silicates. This result was combined with the O–O and Si–Si distances from the first two peaks in the pair distribution functions to show that there are rigid-unit rotations of the SiO$_4$ tetrahedra such that the Si–O–Si angle is bent towards 145–150° rather than the linear bond suggested by the ideal structure. The *second* important result was that the pair distribution functions for the β- and α-phases of cristobalite differ for distances greater than 5 Å, which implies that the structures of the two phases are only the same over the distance scale of a single SiO$_4$ tetrahedron. This result suggested that the model of the structure of β-cristobalite being composed of domains of α-cristobalite is not appropriate.

In this paper we present a new analysis of these earlier neutron $S(Q)$ data, using a new form of the 'reverse Monte Carlo' (RMC) method [22–27]. The idea is that the atoms in a configuration are moved by a Monte Carlo method to give a final configuration that reproduces the experimental data. In the simplest implementation, the only data are for $S(Q)$ or the pair distribution function. This approach was modified to allow for the use of constraints [24, 25]. The important constraints for studies of silica are on the Si–O bond length and the O–Si–O angle. The latter constraint ensures the integrity of the SiO$_4$ tetrahedra, and the former constraint is set by the distances given by the pair distribution functions. More recently we have added a new constraint by including the intensities of the Bragg peaks as a distinct set of data [26, 27]. There are two important effects of this. One is that the Bragg intensities give a constraint on the long-range order of the RMC configuration (at least within the length scale of the RMC simulation). This constraint balances the short-range order that the RMC gives through the constraints from the pair distribution function, and this allows the RMC analysis to give simultaneous information about both the long-range and short-range order. The second effect is that the Bragg peaks give information about the three-dimensional structure through their dependence on (h, k, ℓ).

From the RMC configurations it is possible to calculate any distribution function. Our main objective is to use the RMC method to examine the structures of the two phases of cristobalite through calculations of appropriate distribution functions. In this study we will search for any evidence that the domain model may be in any way appropriate, and we will investigate other structural models of the disorder. We will also investigate any temperature dependence in the β-phase, and compare the degree of disorder in the two phases.

2. Methods and analysis

2.1. Experimental methods

The measurements of the neutron total scattering function $S(Q)$ were performed on powdered samples of cristobalite using the LAD diffractometer (now decommissioned) at the ISIS pulsed spallation neutron source [28]. LAD was a time-of-flight diffractometer, with measurements carried out using banks of detectors covering a wide range of scattering angles in order to give a wide coverage of the scattering vector Q.

The sample of cristobalite used in the experiment was obtained by annealing silica glass at 1600 °C for six days (note that there is a typographical error on this detail in [10]). The sample volume was about 3 cm^3. Other details of the measurements are given in our earlier paper [10]. These include details of the standard procedures [18, 19, 30] that we followed to correct the data for the effects of background scattering, scattering from the vanadium sample can, and absorption and attenuation of the neutron beam, and to normalize the data in order to produce an absolute measurements of $S(Q)$ for values of Q between 0.5 and 50 Å^{-1}. Data were collected for five temperatures, one (475 K) in the α-phase and four (575, 700, 825, 950 K) in the β-phase.

2.2. Total scattering correlation functions

The scattering function can be written in the following form [29]:

$$S(Q) = \frac{1}{N}\frac{d\sigma}{d\Omega} = F(Q) + \sum_{i=1}^{N} c_i \overline{b_i^2} \tag{1}$$

where $4\pi \sum_i c_i \overline{b_i^2}$ is the total scattering cross section of the material, and the summation is over the n atom types. There are N atoms in the material, and c_i gives the proportion of atom type i. $\overline{b}_i$ is the coherent scattering length of atom type i. $F(Q)$ is related to the total radial distribution function $G(r)$ by the Fourier transform

$$F(Q) = \rho_o \int_0^\infty 4\pi r^2 G(r) \frac{\sin Qr}{Qr} \, dr \tag{2}$$

where $G(r)$ is defined as

$$G(r) = \sum_{i,j} c_i c_j \overline{b}_i \overline{b}_j \left[g_{ij}(r) - 1 \right] \tag{3}$$

and $4\pi r^2 \rho_j g_{ij}(r) \, dr$ is the number of atoms of type j lying within a spherical shell of inner and outer radii r and $r + dr$ surrounding an atom of type i. ρ_j is the number of atoms of type j per unit volume, and is equal to $c_j \rho_0$, where ρ_0 is the overall number density. By definition, $G(r) \to 0$ as $r \to \infty$.

$G(r)$ is obtained from experimental data through the inverse transform

$$G(r) = \frac{1}{(2\pi)^3 \rho_0} \int_0^\infty 4\pi Q^2 F(Q) \frac{\sin Qr}{Qr} \, dQ. \tag{4}$$

Combining this with equation (2), we see that the quantities related by the transforms are $QF(Q)$ and $rG(r)$. For this reason, it is appropriate to present the pair distribution functions in terms of the function

$$D(r) = 4\pi \rho_0 r G(r). \tag{5}$$

In the same spirit, we can define corresponding functions for individual atom pairs:

$$d_{ij}(r) = r\left[g_{ij}(r) - 1\right]. \tag{6}$$

From equation (4), $G(r)$ is equal to $-(\sum_i c_i \bar{b}_i)^2$ in the limit $r \to 0$, which means that $D(r)$ has a negative linear form at small r. For this reason, it is common to use the function

$$T(r) = D(r) + 4\pi\rho_0 r \left(\sum_i c_i \bar{b}_i\right)^2 \tag{7}$$

to describe the pair correlations at small distances. The advantage is that when the peaks in $T(r)$ do not overlap, they lie on a background term of zero value (aside from any noise), whereas the low-r peaks in $D(r)$ lie on a negative sloping background [18, 19].

2.3. Preliminary data analysis

The $F(Q)$ data were converted to $G(r)$ using an inverse Monte Carlo method [35]. This has the main advantage of reducing the termination ripples that arise from a standard Fourier transform. In figure 2 we show the $QF(Q)$ data for cristobalite at all of the temperatures of the measurements, and in figure 3 we show the corresponding transforms to $T(r)/4\pi\rho_0$. The peaks in $T(r)$ correspond to specific interatomic distances, and in figure 3 we mark the peaks corresponding to the Si–O and O–O bonds within the SiO$_4$ tetrahedra.
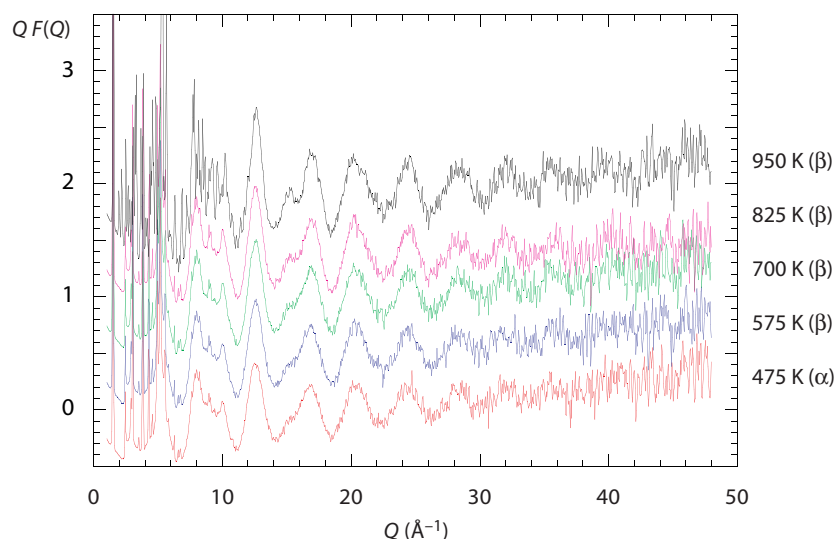

Figure 2. Measurements of $QF(Q)$ for cristobalite at five temperatures, with the data from successive temperatures shifted by a vertical offset for clarity. The large scatter of the data at high values of Q arises because of the factor of Q. The sharp peaks at the lower values of Q are the Bragg peaks.

In addition to converting the data to $F(Q)$, we also converted the data into a form suitable for Rietveld analysis and for extraction of the intensities of Bragg peaks. Both procedures were performed using the CCSL code developed at ISIS [31, 32]. The intensities of the Bragg peaks, which are required for the RMC modelling, were extracted from the diffraction data using the Pawley method [33]. The Rietveld analysis gave accurate lattice parameters needed for the RMC modelling.
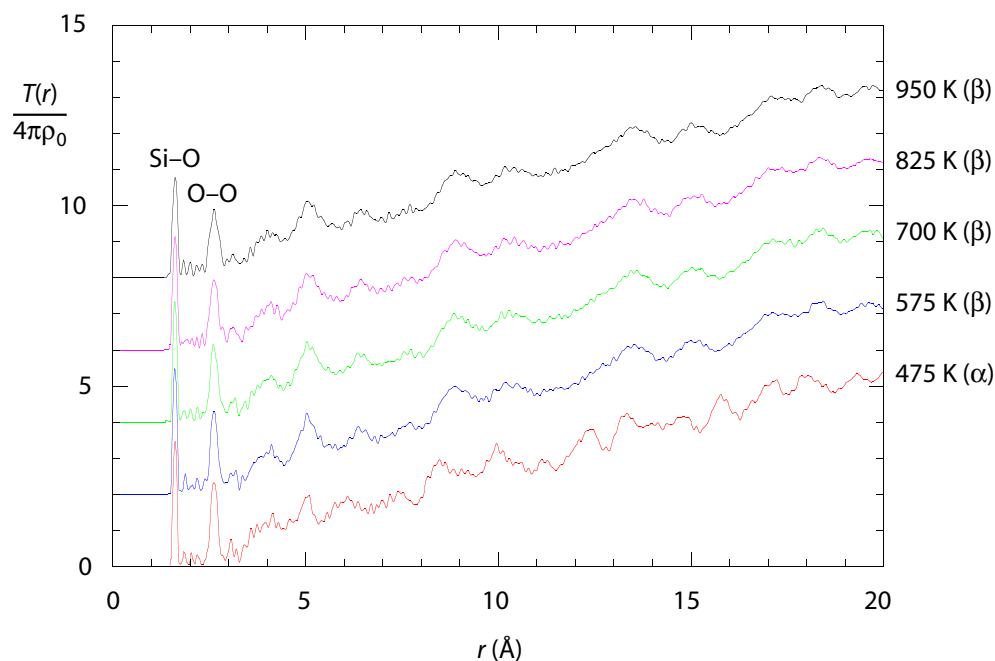
Figure 3. Functions $T(r)/4\pi\rho_0$ for cristobalite at five temperatures, obtained by Fourier transformation of the data shown in figure 2. The two peaks at the lowest distances r correspond to the Si–O and O–O bonds. Data from successive temperatures have been shifted by a vertical offset for clarity.

2.4. Rietveld analysis

The Rietveld refinements were performed using two models for the structure of the β-phase. The first was the idealized model with O atoms on position $(0, 0, 0)$ and Si atoms on position $(1/8, 1/8, 1/8)$ (the setting of the space group $Fd\bar{3}m$ has the centre of symmetry on the origin), and the second was a six-site model for the oxygen atoms, with positions $(0, y, y)$. In the refinements of both models, and for the α-phase, anisotropic temperature factors were refined along with the lattice parameters, atomic coordinates, and background. In table 1 we give the main results from these refinements, which compare well with earlier Rietveld refinements from neutron powder diffraction data [6]. The fitted diffraction patterns for the two phases of cristobalite are shown in figure 4.

The refined structures of the two models for β-cristobalite are shown with thermal ellipsoids in figure 1. The interesting point seen in figure 1 is that in the six-site model the thermal displacement ellipsoids of the oxygen atoms in the small rings overlap, giving the possibility of a continuous distribution of oxygen atoms around an annulus rather than a strict localization over six specific sites.

In table 1 we show the distances between the refined positions of neighbouring Si and O atoms (often taken to approximate the Si–O bond lengths) given by the coordinates of the six-site model, and compare these with the actual Si–O bond lengths obtained from the $T(r)$ data. By contrast, the distances between the Si and O positions in the ideal model are equal to $\sqrt{3}a/8$, and are significantly shorter than the Si–O distances from $T(r)$ and those from the six-site model. It can be seen that the Si–O distances from the six-site model are close to the Si–O bond lengths from the $T(r)$ data (figure 3), but are slightly shorter and appear to get

Table 1. Summary of results of the Rietveld refinements of the structure of β-cristobalite using the six-site model, and of α-cristobalite. Standard deviations on the last digits are given in brackets.

β				
T (K)	a (Å)	O(y)	Si–O$_{\text{Rietveld}}$	Si–O$_{T(r)}$
575	7.13101(2)	0.0450(4)	1.609(3)	1.611(2)
700	7.13681(2)	0.0443(4)	1.608(3)	1.612(1)
825	7.14062(2)	0.0418(8)	1.603(6)	1.613(1)
950	7.14353(2)	0.0418(1)	1.604(1)	1.615(2)

α					
a (Å)	c (Å)	Si(x)	O(x)	O(y)	O(z)
4.98645(2)	6.96765(4)	0.2958(1)	0.2403(2)	0.0963(1)	0.17436(8)
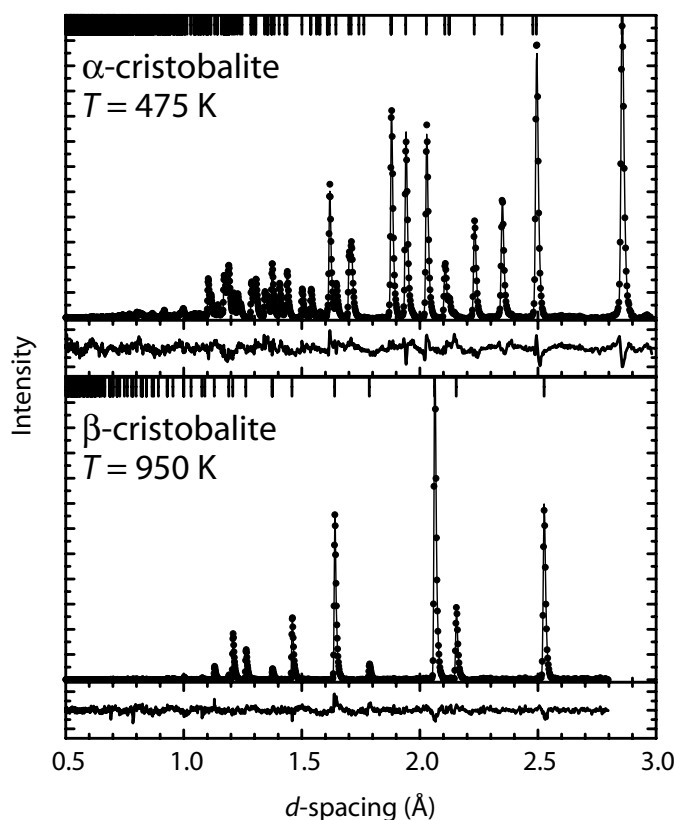
Figure 4. Two examples of the Rietveld fitting to the diffraction data. The vertical bars along the top of each plot represent the d-spacings of the Bragg peaks. The bottom curve in each case represents the difference between the calculated and experimental diffraction patterns scaled by the standard deviation of each point.

even shorter on heating (the apparent coefficient of thermal expansion is -1.0×10^{-5} K^{-1}). This behaviour is a consequence of the fact that the distances between mean positions do not account for correlated fluctuations such as fluctuations in the orientations of the Si–O bond. The normal thermal expansion of the Si–O bond as obtained from $S(Q)$ data (coefficient $(2.2 \pm 0.4) \times 10^{-6}$ K^{-1}) has been discussed previously [34].

2.5. Reverse Monte Carlo modelling

The reverse Monte Carlo (RMC) method [22, 23] as used in this work has been described in detail in previous publications [24, 25]. The idea is to use a Monte Carlo procedure to modify the positions of the atoms in an ensemble. Random changes of the atomic positions are proposed, and are moved subject to the usual rules of the Monte Carlo method as regards changes in the energy function, which is defined as

$$\chi^2 = \sum_j \left| F_{\text{calc}}(Q_i) - F_{\text{exp}}(Q_i) \right|^2 / \sigma_F^2(Q_j) + \sum_j \left| G_{\text{calc}}(r_i) - G_{\text{exp}}(r_i) \right|^2 / \sigma_G^2(r_j)$$

$$+ \sum_{\text{Si–O}} |r_{\text{Si–O}} - R_{\text{Si–O}}|^2 / \sigma_{\text{Si–O}}^2 + \sum_{\text{O–Si–O}} |\theta_{\text{O–Si–O}} - \Theta_{\text{O–Si–O}}|^2 / \sigma_{\text{O–Si–O}}^2$$

$$+ \left| \sum_{hk\ell} |F(hk\ell)|^2_{\text{calc}} - s|F(hk\ell)|^2_{\text{exp}} \right|^2 \Bigg/ \sigma_{hk\ell}^2. \tag{8}$$

The first two terms are the conventional terms in an RMC simulation. In principle these two functions contain the same information, but using the two functions simultaneously picks out different features of the data. The $G(r)$ functions are calculated directly in the simulation, and the $F(Q)$ functions are obtained by Fourier transform. However, if the shortest edge of the simulation sample has length L, $G(r)$ can only be defined up to distance $L/2$. Thus the calculated $F(Q)$ will contain truncation ripples. In order to make a valid comparison with the experimental data, the experimental $F(Q)$ are convoluted with the sinc function:

$$F_{\text{exp}}^{\text{conv}}(Q) = \frac{1}{\pi} \int_{-\infty}^{+\infty} F_{\text{exp}}(Q') \frac{\sin((Q - Q')L/2)}{Q - Q'} \, \mathrm{d}Q'. \tag{9}$$

The weighting parameters σ in equation (8) are allowed to vary from point to point, but in practice constant values are used for all points in both functions.

The third and fourth terms ensure that the SiO_4 tetrahedra retain their size, shape, and integrity, and also ensure that the initial network of SiO_4 tetrahedra is maintained in the RMC simulation. The Si–O distance $r_{\text{Si–O}}$ is allowed to vary around the set value $R_{\text{Si–O}}$, which is chosen to be the position of the peak in $T(r)$ corresponding to the Si–O bond length. The O–Si–O angle $\theta_{\text{O–Si–O}}$ is also allowed to vary around the set point $\Theta_{\text{O–Si–O}} = 109.47°$.

The last term in the RMC energy function is a new addition in our recent work. The functions $F(hk\ell)$ are the crystallographic structure factors of the Bragg peaks, defined at $Q_{hk\ell} = h\boldsymbol{a}^* + k\boldsymbol{b}^* + \ell\boldsymbol{c}^*$:

$$F(hk\ell) = \frac{1}{2\pi N} \sum_j \overline{b}_j \exp(i\boldsymbol{Q}_{hk\ell} \cdot \boldsymbol{r}_j). \tag{10}$$

s is a scale factor, which is obtained by minimization of χ^2:

$$s = \left(\sum_{hk\ell} |F(hk\ell)|^2_{\text{calc}} |F(hk\ell)|^2_{\text{exp}} / \sigma_{hk\ell}^2 \right) \Bigg/ \left(\sum_{hk\ell} |F(hk\ell)|^4_{\text{calc}} / \sigma_{hk\ell}^2 \right). \tag{11}$$

Although the Bragg peaks are included in the total scattering data, and therefore have an impact in the first two terms of χ^2, their effects in these terms are reduced. As far as the $F(Q)$ data are concerned, since the experimental data are broadened by the convolution with the sinc function, the information about the long-range order is reduced. Moreover, in the analysis of $G(r)$ no explicit account is taken of the specific $hk\ell$ indices assigned to the Bragg peaks. As far as the $G(r)$ data are concerned, the information about mean atomic positions gets lost beyond the distance at which there is a large overlap of atomic separations.

As we mentioned above, there are two main purposes of the new term containing the Bragg peak intensities. The first is to ensure that the configuration produced by the RMC simulation is consistent with the long-range order of the experimental system. Since the RMC method is essentially a statistical mechanics method, it will automatically maximize the entropy to produce configurations that are as disordered as possible whilst remaining consistent with the experimental data. The Bragg intensities provide information about the long-range order, and act as an effective constraint on the extent of the disorder that can be generated in the RMC simulation. The second purpose of the use of the Bragg intensities is to provide some degree of the three-dimensional structure. Although the diffraction data are one dimensional, the extracted Bragg peaks are identified with the three-dimensional vectors $Q_{hk\ell}$, providing information about the three-dimensional aspects of the structure as in single-crystal diffraction. In practice the use of the Bragg peaks may or may not have a significant effect on the RMC configurations, but they will certainly increase the confidence in the reliability of the RMC configurations.

As has been noted before [25], because we are refining an initial structure and incorporating constraints that prohibit major changes from the initial structure, our use of the RMC method is more in the line of a tool for *refining* a model than the usual use of *constructing* a model.

The RMC configurations used in our work contained 24 000 or 12 000 atoms for the cubic or tetragonal structures respectively, with initial configurations in either the tetragonal or cubic structures. In both cases the simulation sample corresponded to a $10 \times 10 \times 10$ supercell of the conventional unit cells. The lattice parameters were those given by the Rietveld refinements. In the first stage of the RMC analysis, the energy function only contained the two terms that act as constraints on the Si–O distance and O–Si–O angle. The point of this is to allow the structure to evolve to give the correct bond lengths as the first stage in the model refinement. The $F(Q)$, $G(r)$ and Bragg peak data were then included in the RMC refinement.

3. Results from the RMC analysis

3.1. Atomic configurations

The structure plot shown in figure 1 gives the impression of a continuous distribution of oxygen positions, with tetrahedra tilted by large angles (15–20°) from the orientations of the average positions. How this is realized can be seen in pictures of configurations of the atoms. (111) layers of the configurations of β-cristobalite obtained in the RMC simulations are shown in figure 5, together with a corresponding layer ((201)) from the RMC simulation of α-cristobalite. In the ideal structure of β-cristobalite, the rings of SiO_4 tetrahedra would be perfect hexagons. The large distortions of the rings due to rigid-body rotations and displacements of the tetrahedra can be seen at each of the four temperatures of the β-phase. The RMC configurations of β-cristobalite show no obvious signs of the existence of any domains of whatever structure— the distortions of the hexagonal rings show no spatial correlations. More quantitative analysis in support of this point will be given below, but one might expect that if any domain structure were present it *ought* to be possible to detect it from visual inspection of the configurations. It is quite possible that there are structural correlations involving fluctuations with wave vectors spread across reciprocal space. This is the interpretation of the RUM model (discussed below), and we will show the reciprocal-space analysis later.

The RMC configuration for α-cristobalite shown in figure 5 shows the change in order associated with the phase transition. The figure shows the ideal structure obtained from Rietveld refinement (average structure, with no thermal motion represented). Although the
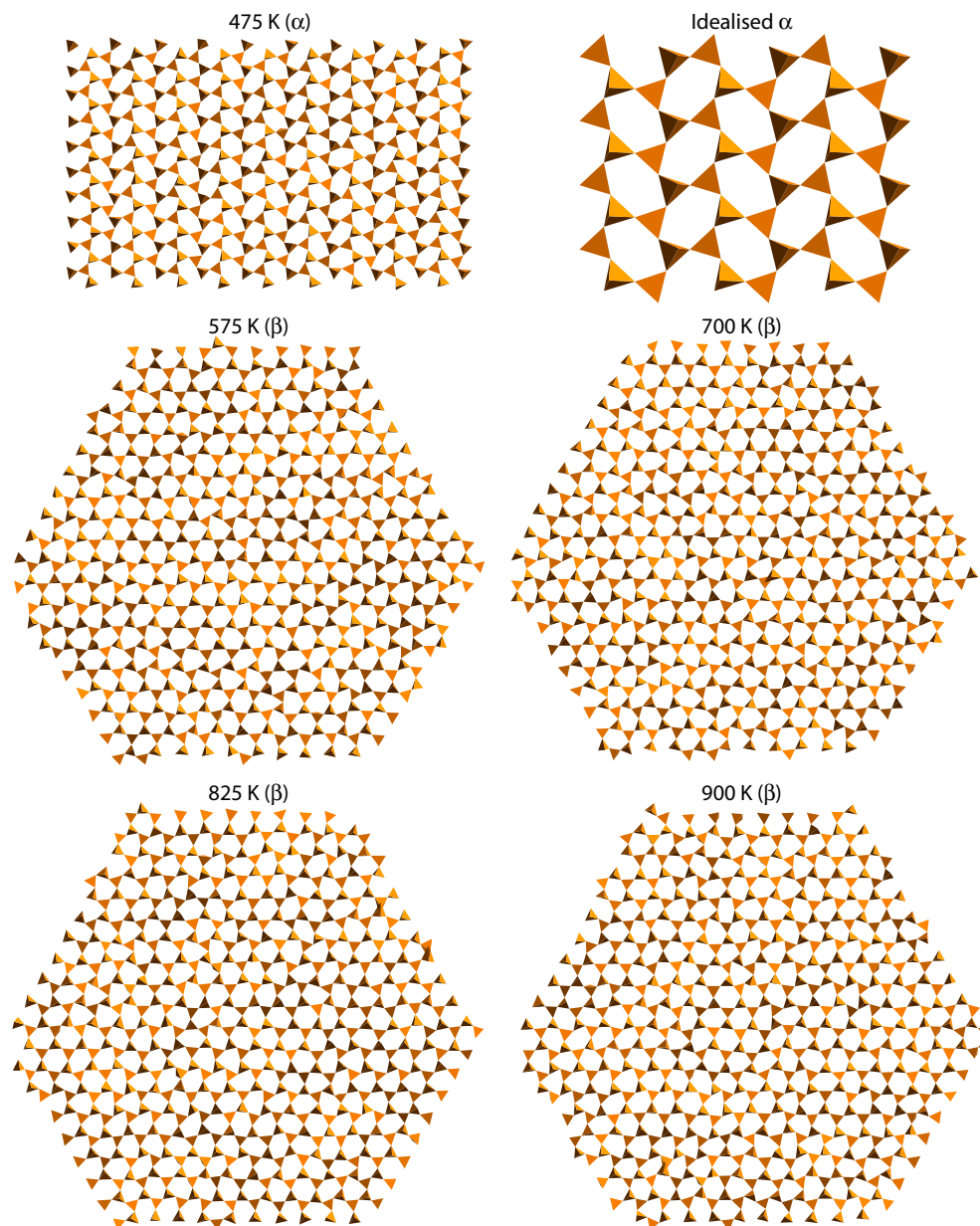
Figure 5. Atomic configurations of cristobalite at the five temperatures obtained from the RMC refinement, with the atoms represented as shaded SiO$_4$ tetrahedra. The views are down the [111] axes of the cubic β-phase, and down the corresponding [201] axis of the tetragonal phase. The figure also shows the corresponding projection of the ideal tetragonal phase with no thermal motion.

order in the structure is clear to see, it is also clear that there is still a significant amount of orientational disorder.

In the following sections we provide a number of quantitative evaluations of the structural disorder.

3.2. Pair distribution functions

Earlier we drew attention to the $T(r)$ data shown in Figure 3. We noted in our previous publication [10] that the $T(r)$ functions for all temperatures in the β-phase are very similar, but there are differences in the $T(r)$ functions between the α- and β-phases for distances beyond 5 Å. These differences are highlighted in calculations of the individual pair distribution functions $d_{ij}(r)$ from the RMC configurations shown in figure 6.
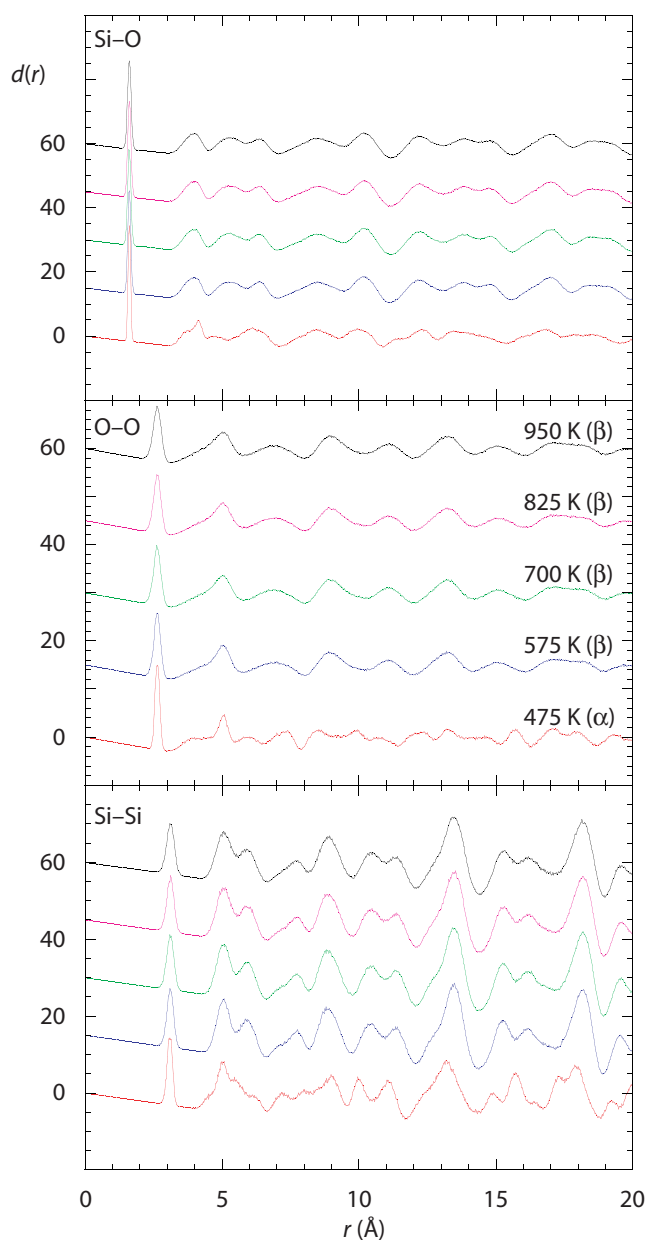

Figure 6. Calculated $d_{ij}(r)$ functions for cristobalite at the five temperatures, obtained from the RMC refinement. The data for each temperature are shifted by a vertical offset for clarity.

We note from the outset that the Si–Si pair distribution function has little effect on the overall $T(r)$. This is due to the weaker scattering lengths of the Si atoms and the small proportion of Si atoms. The strongest peak in $d_{Si-Si}(r)$ is the nearest-neighbour peak at ~ 3.1 Å, which shows as an extremely weak feature in the $T(r)$ data of figure 3. Thus the peaks in the $T(r)$ data of β-cristobalite at ~ 5 Å can be identified with peaks in $d_{O-O}(r)$, and the peaks in the $T(r)$ data of β-cristobalite at ~ 4, ~ 6.5, and ~ 10 Å can be identified with peaks in $d_{Si-O}(r)$, and the peaks in the $T(r)$ data at ~ 9 Å can be identified with peaks in both $d_{O-O}(r)$ and $d_{Si-O}(r)$. The most significant changes in the individual pair distribution functions between α-cristobalite and β-cristobalite over the range 5–10 Å occur in $d_{O-O}(r)$, and these changes almost account for all of the differences between the $T(r)$ functions shown in figure 3 and discussed in some detail in [10]. There are slight changes in $d_{Si-Si}(r)$, due to the changes in the lattice parameters and small symmetry-breaking displacements of the SiO$_4$ tetrahedra, and in $d_{Si-O}(r)$. It is not at all surprising that the most significant changes between the two phases are in $d_{O-O}(r)$, because the displacive phase transition is primarily associated with changes in the orientations of the SiO$_4$ tetrahedra, with only small symmetry-breaking displacements of the Si cations.

3.3. Bond-angle distribution functions

Figure 7 shows the distribution functions for the O–Si–O, Si–O–Si and Si–Si–Si bond angles, plotted as functions of $\cos\theta$, where θ represents the particular bond angle. The O–Si–O angle distribution function (ADF) is expected to have a peak around the tetrahedral angle $\cos^{-1}(-1/3) = 109.47°$, which is indeed found to be the case. The breadth of this peak reflects the extent to which the tetrahedra are distorted. It is striking that this distribution is somewhat broader in the β-phase than in the α-phase—more than can be accounted for by simple thermal motion (the pure effects of thermal motion can be seen by comparing the ADFs for the four temperatures of the β-phase). It is clear that the large-amplitude rotations of the SiO$_4$ tetrahedra that characterize the disorder in the β-phase are accompanied by small distortions of the angles within the SiO$_4$ tetrahedra. Our earlier analysis of the $T(r)$ data [10,34] showed that there are no corresponding changes in the Si–O bond lengths.

The Si–O–Si ADF for β-cristobalite is a broad single peak centred on $\cos\theta = -1$, but for α-cristobalite the ADF has a maximum at $\cos\theta = -0.85$, which corresponds to a most probable Si–O–Si angle of 148°. This difference is actually a little misleading. The corresponding distribution function in terms of the bond angle, $P(\theta)$, is related to the distribution function in terms of $\cos\theta$ by $P(\theta) = P(\cos\theta)\sin\theta$. This means that the peak in $P(\cos\theta)$ at $\cos\theta = -1$ actually corresponds to a value of zero in $P(\theta)$. Thus the Si–O–Si ADF for β-cristobalite is showing a broad peak at slightly larger angles as compared to that in α-cristobalite. This comparison will also be seen in the discussion of figure 10 below.

The Si–Si–Si ADF is a broad single-peaked function centred on $\cos^{-1}(-1/3)$ (most probable angle of 109.47°) for β-cristobalite at all temperatures. This is consistent with the average structure, as it is based on the diamond structure with respect to the positions of the Si atoms. However, for α-cristobalite the ADF has three peaks, the strongest being centred on $\cos^{-1}(-1/3)$ and being sharper than for β-cristobalite, with two new outside peaks at $\cos\theta \sim -0.58$ and $\cos\theta \sim -0.05$ which extend beyond the range of the ADF of β-cristobalite. The centres of these two peaks correspond to the angles $\theta = 126°$ and $\theta = 93°$ respectively, which are the values of some of the Si–Si–Si angles in the average crystal structure of α-cristobalite.

The significant differences in the Si–O–Si and Si–Si–Si ADFs between the two phases show that the short-range structures of the two phases are quite different, consistent with the
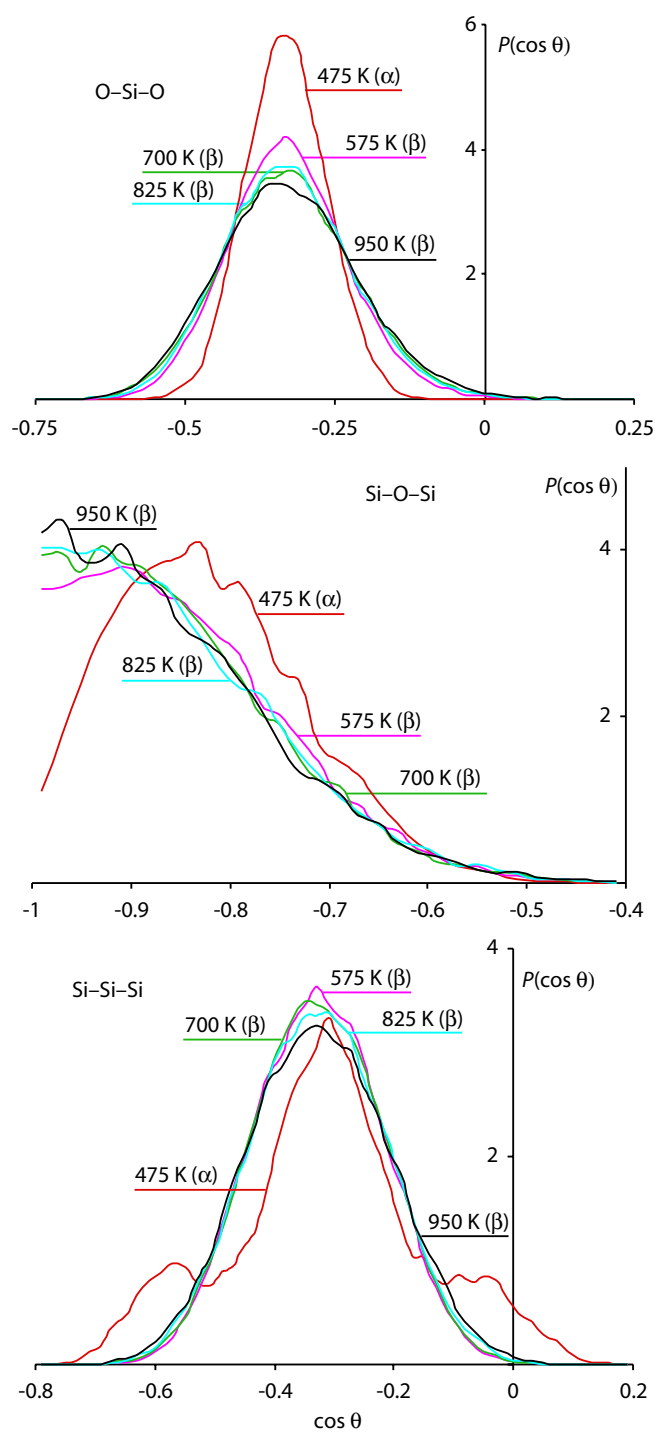
Figure 7. Three bond-angle distribution functions for cristobalite at the five temperatures. In each case, the distribution functions for all temperatures in the β-phase are very similar, but significantly different from the distribution functions of the α-phase. The data are given as functions of $\cos \theta$, where θ is the particular bond angle in each case.

qualitative impressions given by the configurations in figure 5. In particular, the absence of the Si–Si–Si angles at $\theta = 126°$ and $\theta = 93°$ in β-cristobalite shows that any local fluctuations of the structure of β-cristobalite into domains of the structure of α-cristobalite must have low probability.

One important point from the bond angle distribution functions is that although their widths have some temperature dependence in the β-phase, the changes with temperature are substantially smaller than the changes between the α- and β-phases. This clearly shows that there are significant differences between the short-range structures of the two phases, and that the dynamical disorder in the β-phase is more than simple thermal motion. Instead, the orientational disorder that gives rise to the changes in the ADFs is intrinsic to the structure of β-cristobalite.

3.4. Bond correlations

We now search for correlations between different bond angles and between bond angles and distances. The bond angles for this analysis are defined in figure 8. θ is the Si–O–Si angle, and ϕ is the angle between the Si–O–Si plane and any of the O–Si–O planes. In effect, ϕ gives the direction of the tilt of the Si–O–Si bond. r is defined as the length of either of the Si–O bonds in a Si–O–Si linkage. Figure 9 shows two-dimensional maps of the distributions of θ and r, and figure 10 shows the maps of the distributions of θ and ϕ. The θ–r maps show a spread of values of the Si–O–Si angles in accord with the results of the previous discussion (figure 7), together with a spread in values of the Si–O bond length. The shape of the coupled distribution shows no obvious correlation between the two quantities—such a correlation should be indicated if the distribution was in the shape of an ellipse with axes that are not parallel to the axes of the plot. The lack of correlation should be contrasted with the findings from the quantum mechanical
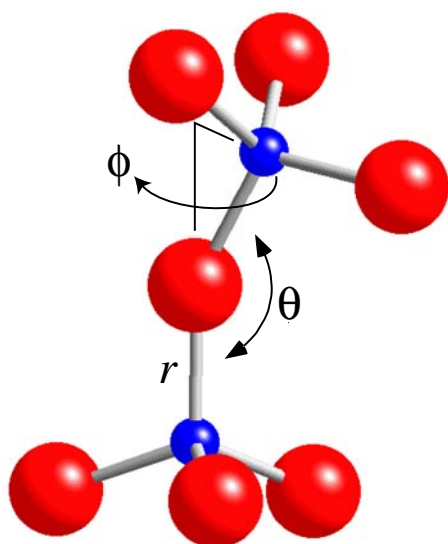

Figure 8. Definitions of the angles associated with the relative orientations of two linked SiO_4 tetrahedra. θ is the Si–O–Si bond angle. ϕ is the angle between the direction of the tilt of the bridging Si–O bond of one tetrahedron projected onto the plane of the three basal oxygen atoms of the other tetrahedron: the value $\phi = 0$ corresponds to the bridging Si–O bond tilting in the direction of one of the basal oxygen atoms.
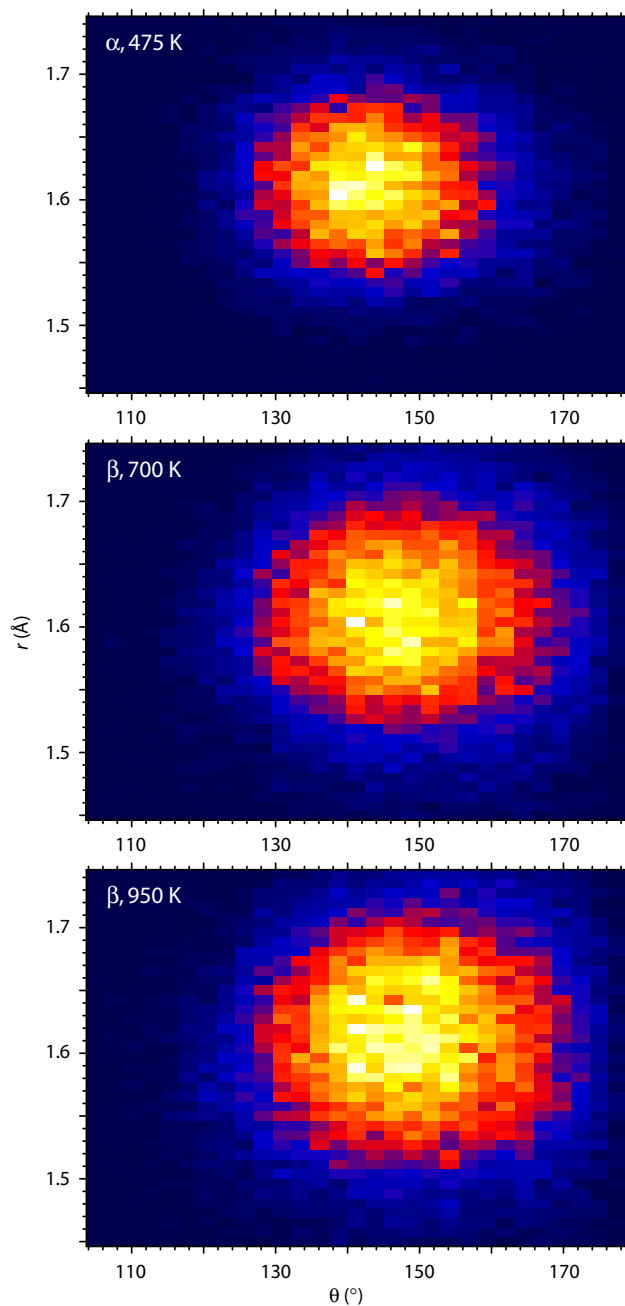
Figure 9. Maps of the distributions of θ (defined in figure 8) and the lengths of either of the two Si–O bonds, r. The higher values of the distributions are indicated by the lighter shading of the map.

calculations of Lasaga and Gibbs [36]. These suggested that an increase of the Si–O–Si angle should be accompanied by a shortening of the Si–O bonds. It is clear that, at least as far as fluctuations in the structure are concerned, there are no clear correlations of this sort.
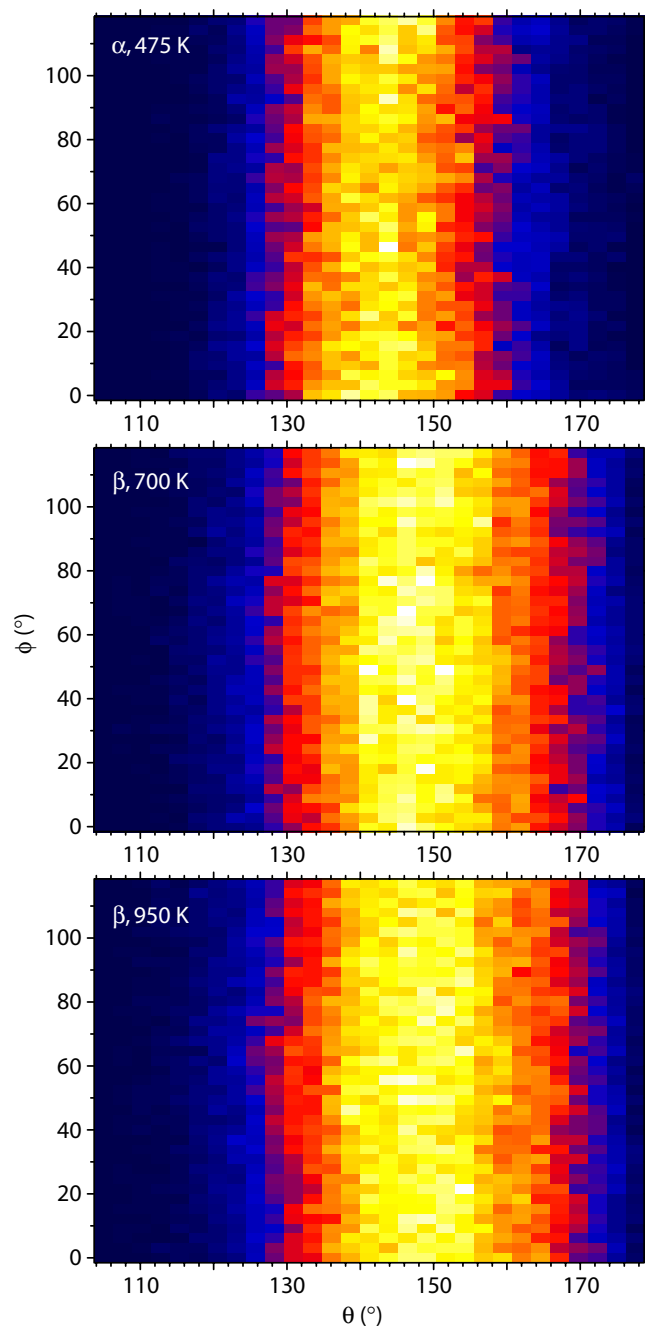
Figure 10. Maps of the distributions of the θ- and ϕ-angles defined in figure 8. The higher values of the distributions are indicated by the lighter shading of the map.

The θ–ϕ plots, figure 10, show that there is a wide distribution of the values of ϕ. This implies that there are no special orientations of the Si–O bond, but that all orientations are likely. Looking back at the plots of the structure of β-cristobalite in figure 1, it is clear that the

six-site model gives probability distribution functions for the positions of the oxygen atoms that overlap, and this overlap is consistent with the continuous distribution in the ϕ-angles seen in figure 10. There is also a broad distribution of the ϕ-angles for α-cristobalite, with some weak structure to the distribution. The average structure has several values of ϕ, and the structural disorder seen in figure 5 simply smears the distributions into broad continuous distributions.

3.5. Calculations of diffuse scattering

It is possible to calculate the three-dimensional diffuse scattering from the atomic configurations generated by the RMC modelling. Specifically, we calculate

$$S(\boldsymbol{Q}) = \sum_{i,j} \overline{b}_i \overline{b}_j \langle \exp(\mathrm{i}\boldsymbol{Q} \cdot [r_i - r_j]) \rangle \tag{12}$$

where r_i is the instantaneous position of the atom with label i, and as before b_i is the corresponding scattering length. Note that we have a grid of values of $\boldsymbol{Q}$ as given by the size of the RMC simulation sample.

Analysis of a single configuration gives relatively noisy results. Therefore in our calculations of $S(\boldsymbol{Q})$ we averaged over symmetry in order to reduce the statistical noise, and used a Gaussian smoothing over neighbouring grid points. The results for the five temperatures are shown in figure 11. The diffuse scattering maps for all temperatures in the β-phase show similar features of lines along $\langle 1, 0, 0 \rangle^*$ and $\langle 1, 1, 0 \rangle^*$. These features reproduce the experimental measurements of diffuse scattering by transmission electron microscopy (TEM), which are also shown in figure 11 [2, 3]. These lines correspond exactly to the RUM calculations [7, 13, 14]. In α-cristobalite, the modes that give the strong diffuse scattering in the cubic phase are no longer RUMs [7, 14]. However, they will still be at reasonably low frequency just below the transition temperature and will therefore give weak 'shadows' of the diffuse scattering of the cubic phase. This is what is seen in the plots in figure 11.

There are two implications of these results. The *first* is that the RMC models have correctly reproduced the real three-dimensional structure and three-dimensional fluctuations. It is perhaps remarkable that it has been possible to accurately construct the three-dimensional diffuse scattering from the one-dimensional powder diffraction data! On the other hand, it is also likely to be true that if the RMC models, including the data-based constraints, have captured the correct physics, they may not have the freedom to do other than reproduce the correct RUM fluctuations that give the experimental diffuse scattering. Thus follows the *second* implication of these results, namely that the configurations produced by RMC modelling are consistent with the ability of the RUMs to generate disorder.

4. Discussion

From the RMC analysis of the neutron total scattering data from cristobalite presented in this paper we can draw a number of conclusions. The most straightforward is that we have further evidence that the structure of β-cristobalite cannot be described in terms of a limited number of domains of an ordered structure. The atomic configurations generated by the RMC analysis, together with the distributions functions and three-dimensional diffuse scattering patterns calculated from these configurations, lend a lot of support to the RUM interpretation of the origin of the structural disorder. The RMC analysis has given more details of the nature of the structural disorder, in particular showing that there are no preferred sites for the oxygen atoms but that instead each oxygen atoms lies on an continuous annulus of possible positions.
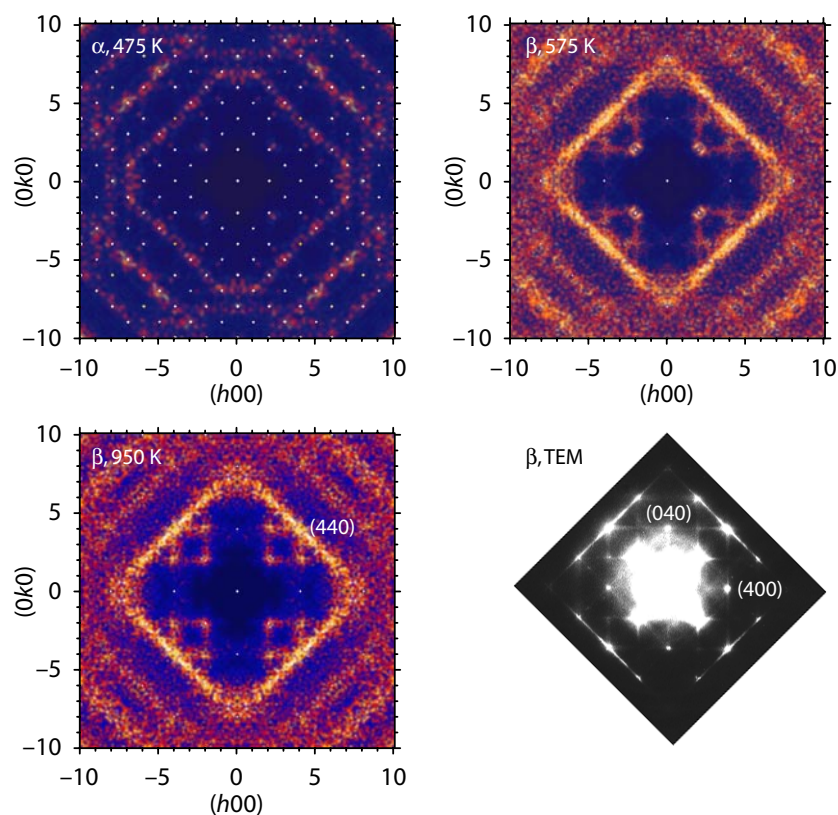
Figure 11. Maps of the three-dimensional diffuse scattering from cristobalite, showing the a^*–b^* plane in reciprocal space. The plot for α-cristobalite is indexed as β-cristobalite in order to highlight the common aspects. The single-pixel white spots are the Bragg peaks. The intensity of the diffuse scattering, as indicated by the shading (light for higher intensity, dark for low intensity) is the same for all plots. The plot in the bottom-right corner shows experimental TEM measurements for β-cristobalite [2].

It should be remarked that it has only been possible to draw this conclusion from the fact that the data extend to a large value of Q_{max}. The distances between the sites in the six-site model are closer than the resolution possible in a normal diffraction experiment, meaning that traditional crystallographic analysis would not easily be able to distinguish between the six-site model and the continuous annulus model.

In the β-phase there is only a small effect of temperature on the structure fluctuations, with the disordered structures being similar for all temperatures. But on cooling through the phase transition, there are changes to the atomic configurations, distribution functions, and structure of the three-dimensional diffuse scattering. However, it is clear from the analysis that there is still considerable structural disorder in the α-phase, even though the phase transition has a large first-order discontinuity.

One interesting result from the RMC analysis is that there appears to be little correlation between the length of an Si–O bond and the corresponding Si–O–Si angle. This correlation had been predicted from quantum mechanical calculations on small silica clusters [36], and at face value appears to hold for experimental structural data such as those for β-cristobalite, where an apparent linear Si–O–Si angle is correlated with an apparently short Si–O bond. However,

such experimental data are not appropriate because, as we see in the case of β-cristobalite, Si–O bonds that appear to be too short are indicative of structural disorder with rotations of longer Si–O bonds. The results of this study show that, at least as far as structural fluctuations are concerned, there are no correlations between the Si–O bond length and the Si–O–Si angle.

We have remarked that the present results are in agreement with the predictions of the RUM model. Moreover, they are also in agreement with recent molecular dynamics simulations (MDS) of a simple model of β-cristobalite [11]. This simple model was designed to most closely approximate the RUM ideas by simulating rigid SiO_4 tetrahedra with linked vertices joined by springs of zero equilibrium length. One of the main results from this model was that the configurations produced by the MDS showed many similarities to the configurations produced by the RMC. The MDS also showed that all RUMs are excited, giving a pattern of diffuse scattering similar to that found in this study. Thus the RMC and MDS results are in close agreement, and both present support for the RUM model of the phase transition and of the nature of the structural disorder in the β-phase. The results for the orientations of the Si–O bond are also in agreement with those from earlier MDS studies using realistic interatomic potentials [8].

Acknowledgment

References

[1] Heaney P J 1994 Structure and chemistry of the low-pressure silica polymorphs *Rev. Mineral.* **29** 1–40

[2] Hua G L, Welberry T R, Withers R L and Thompson J G 1988 An electron-diffraction and lattice-dynamical study of the diffuse scattering in β-cristobalite, SiO_2 *J. Appl. Crystallogr.* **21** 458–65

[3] Welberry T R, Hua G L and Withers R L 1989 An optical transform and Monte Carlo study of the disorder in β-cristobalite SiO_2 *J. Appl. Crystallogr.* **22** 87–95

[4] Withers R L, Thompson J G and Welberry T R 1989 The structure and microstructure of α-cristobalite and its relationship to β-cristobalite *Phys. Chem. Minerals* **16** 517–23

[5] Hatch D M and Ghose S 1991 The α–β phase transition in cristobalite, SiO_2: symmetry analysis, domain structure, and the dynamic nature of the β-phase *Phys. Chem. Minerals* **17** 554–62

[6] Schmahl W W, Swainson I P, Dove M T and Graeme-Barber A 1992 Landau free energy and order parameter behaviour of the α–β phase transition in cristobalite *Z. Kristall.* **201** 125–45

[7] Swainson I P and Dove M T 1993 Low-frequency floppy modes in β-cristobalite *Phys. Rev. Lett.* **71** 193–6

[8] Swainson I P and Dove M T 1995 Molecular dynamics simulation of α- and β-cristobalite *J. Phys.: Condens. Matter* **7** 1771–88

[9] Swainson I P and Dove M T 1995 On the thermal expansion of β-cristobalite *Phys. Chem. Minerals* **22** 61–5

[10] Dove M T, Keen D A, Hannon A C and Swainson I P 1997 Direct measurement of the Si–O bond length and orientational disorder in β-cristobalite *Phys. Chem. Minerals* **24** 311–7

[11] Gambhir M, Dove M T and Heine V 1999 Rigid unit modes and dynamic disorder: SiO_2 cristobalite and quartz *Phys. Chem. Minerals* **26** 484–95

[12] Wright A F and Leadbetter A J 1975 The structures of the β-cristobalite phases of SiO_2 and $AlPO_4$ *Phil. Mag.* **31** 1391–401

[13] Giddy A P, Dove M T, Pawley G S and Heine V 1993 The determination of rigid unit modes as potential soft modes for displacive phase transitions in framework crystal structures *Acta Crystallogr.* A **49** 697–703

[14] Hammonds K D, Dove M T, Giddy A P, Heine V and Winkler B 1996 Rigid unit phonon modes and structural phase transitions in framework silicates *Am. Mineral.* **81** 1057–79

[15] Dove M T 1997 Theory of displacive phase transitions in minerals *Am. Mineral.* **82** 213–44

[16] Dove M T, Heine V, Hammonds K D, Gambhir M and Pryde A K A 1998 Short-range disorder and long-range order: implications of the 'rigid unit mode' model *Local Structure From Diffraction* ed M F Thorpe and S Billinge (New York: Plenum) pp 253–72

[17] Hammonds K D, Dove M T, Giddy A P and Heine V 1994 CRUSH: a FORTRAN program for the analysis of the rigid unit mode spectrum of a framework structure *Am. Mineral.* **79** 1207–9

[18] Wright A C 1993 Neutron and x-ray amorphography experimental techniques of glass science *Ceramic Transactions* ed C J Simmons and O H El-Bayoumi (Websterville, VT: American Ceramic Society) pp 205–314

[19] Wright A C 1997 X-ray and neutron diffraction: experimental techniques and data analysis *Amorphous Insulators and Semiconductors* ed M F Thorpe and M I Mitkova (Dordrecht: Kluwer) pp 83–131

[20] Keen D A and Dove M T 1999 Comparing the local structures of amorphous and crystalline polymorphs of silica *J. Phys.: Condens. Matter* **11** 9263–73

[21] Keen D A and Dove M T 2000 Total scattering studies of silica polymorphs: similarities in glass and disordered crystalline local structure *Mineral. Mag.* **64** 229–39

[22] McGreevy R L and Pusztai L 1988 Reverse Monte Carlo simulation: a new technique for the determination of disordered structures *Mol. Simul.* **1** 359–67

[23] McGreevy R L 1995 RMC—progress, problems and prospects *Nucl. Instrum. Methods* A **354** 1–16

[24] Keen D A 1997 Refining disordered structural models using reverse Monte Carlo methods: application to vitreous silica *Phase Transitions* **61** 109–24

[25] Keen D A 1998 Reverse Monte Carlo refinement of disordered silica phases *Local Structure From Diffraction* ed M F Thorpe and S J L Billinge (New York: Plenum) pp 101–19

[26] Tucker M G, Dove M T and Keen D A 2000 Simultaneous measurements of changes in long-range and short-range structural order at the displacive phase transition in quartz *J. Phys.: Condens. Matter* **12** L723–30

[27] Tucker M G, Dove M T and Keen D A 2001 Application of the reverse Monte Carlo method to crystalline materials. *J. Appl. Crystallogr.* submitted

[28] Howells W S and Hannon A C 1999 LAD, 1982–1998: the first ISIS diffractometer *J. Phys.: Condens. Matter* **11** 9127–38

[29] Keen D A 2001 A comparison of various commonly used correlation functions for describing total scattering *J. Appl. Crystallogr.* submitted

[30] Howe M A, McGreevy R L and Howells W S 1989 The analysis of liquid structure data from time-of-flight neutron diffractometry *J. Phys.: Condens. Matter* **1** 3433–51

[31] Brown P J and Matthewman J C 1987 *Rutherford Appleton Laboratory Report* RAL-87-010

[32] David W I F, Ibberson R M and Matthewman J C 1992 *Rutherford Appleton Laboratory Report* RAL-92-032

[33] Pawley G S 1981 Unit-cell refinement from powder diffraction scans *J. Appl. Crystallogr.* **14** 357–61

[34] Tucker M G, Dove M T and Keen D A 2000 Direct measurement of the thermal expansion of the Si–O bond by neutron total scattering *J. Phys.: Condens. Matter* **12** L425–30

[35] Pusztai L and McGreevy R L 1997 MCGR: an inverse method for deriving the pair correlation function from the structure factor *Physica* B **234–236** 357–8

[36] Lasaga A C and Gibbs G V 1991 Quantum-mechanical Hartree–Fock potential surfaces and calculations on minerals 2. 6-31 G* results *Phys. Chem. Minerals* **17** 485–91